Niche-specific macrophage loss promotes skin capillary aging

Kailin R. Mesa[1*], Kevin A. O'Connor[1], Charles Ng[2], Steven P. Salvatore[2], Dan R. Littman[1,3,4*]

[1] Department of Cell Biology, New York University School of Medicine, New York, NY 10016, USA
[2] Department of Pathology and Laboratory Medicine, Weill Cornell Medicine, New York-Presbyterian Hospital, New York, NY 10021, USA
[3] Perlmutter Cancer Center, New York University Langone Health, New York, NY 10016, USA
[4] Howard Hughes Medical Institute, New York, NY 10016, USA

* To whom correspondence should be addressed

Email: kai.mesa@med.nyu.edu or dan.littman@med.nyu.edu
Tel: 212-263-7520

Key Words: Aging / Resident Macrophages / Blood Capillaries / Tissue Repair / Intravital Microscopy

Running Title: Niche-specific macrophage loss promotes capillary aging

Summary

All mammalian organs depend upon resident macrophage populations to coordinate repair processes and facilitate tissue-specific functions[1–3]. Recent work has established that functionally distinct macrophage populations reside in discrete tissue niches and are replenished through some combination of local proliferation and monocyte recruitment[4,5]. Moreover, decline in macrophage abundance and function in tissues has been shown to contribute to many age-associated pathologies, such as atherosclerosis, cancer, and neurodegeneration[6–8]. Despite these advances, the cellular mechanisms that coordinate macrophage organization and replenishment within an aging tissue niche remain largely unknown. Here we show that capillary-associated macrophages (CAMs) are selectively lost over time, which contributes to impaired vascular repair and tissue perfusion in older mice. To investigate resident macrophage behavior *in vivo*, we have employed intravital two-photon microscopy to non-invasively image in live mice the skin capillary plexus, a spatially well-defined model of niche aging that undergoes rarefication and functional decline with age. We find that CAMs are lost with age at a rate that outpaces that of capillary loss, leading to the progressive accumulation of capillary niches without an associated macrophage in both mice and humans. Phagocytic activity of CAMs was locally required to repair obstructed capillary blood flow, leaving macrophage-less niches selectively vulnerable to both homeostatic and injury-induced loss in blood flow. Our work demonstrates that homeostatic renewal of resident macrophages is not as finely tuned as has been previously suggested[9–11]. Specifically, we found that neighboring macrophages do not proliferate or reorganize sufficiently to maintain an optimal population across the skin

capillary niche in the absence of additional cues from acute tissue damage or increased abundance of growth factors, such as colony stimulating factor 1 (CSF1). Such limitations in homeostatic renewal and organization of various niche-resident cell types are potentially early contributors to tissue aging, which may provide novel opportunities for future therapeutic interventions.

Main Text

Tissue homeostasis is dependent on multiple macrophage populations that reside in distinct sub-tissue compartments or niches, such as epithelium, blood vessels or nerves, and are thought to support specialized tissue functions[4,12,13]. Recent work has suggested that functional decline and rarefication of vascular niches may contribute to various age-associated tissue pathologies (including sarcopenia, chonic wounds, and Alzheimer's disease)[14–16]. It is not yet known how tissue-resident macrophages resist or potentiate such niche specific aging processes[6,17].

Capillary-associated macrophage decline with age correlates with impaired blood flow.

To model mammalian tissue aging, we adapted an intravital microscopy technique to visualize skin resident macrophage populations non-invasively in live mice throughout the lifetime of the organism[18,19] (Figure 1a, Supplemental Videos 1 and 2). Unexpectedly, longitudinal imaging of skin macrophages (marked by *Csf1r-EGFP*) revealed niche-specific decline in macrophage populations. Subdividing the skin into

three anatomical layers, epidermis, upper (papillary) and lower (reticulated) dermis, we observed that macrophages of the upper dermis were lost with age at a greater rate than macrophages from both epidermis and lower dermis (Figure 1b-c). Further characterization of this population with additional myeloid fluorescent reporters revealed that most macrophages of the upper dermis express the chemokine receptor CX_3CR1, but not CCR2 (Extended Data Fig. 1a,b). A major component of the upper dermal niche is the superficial capillary plexus, which supplies nutrient exchange for the overlying epidermis. To visualize this structure, we utilized third harmonic generation from our imaging to track red blood cell (RBC) flow[20,21], which was consistent with conventional labeling methods such as rhodamine dextran injection (Extended Data Fig. 1c-e and Supplemental Video 3). With this *in vivo* marker of blood flow, we found that the macrophages were closely associated with blood capillaries of the superficial plexus, suggesting that they may provide support for this capillary niche (Extended Data Fig. 1f-h and Supplemental Video 4). To investigate if these macrophages play a role in capillary function, we assessed if blood flow, via RBC flow (Extended Data Fig. 2), was altered in the presence of capillary-associated macrophages (CAMs). Performing timelapse recordings of fluorescently labeled CAMs in mice with a cre-dependent dual reporter system (*Cx3cr1-CreERT2; R26-mTmG*), we found that capillaries lacking an associated macrophage had a higher rate of obstructed blood flow (Figure 1d,e and Supplemental Video 5). Longitudinal imaging across multiple ages showed that the fraction of capillaries with CAMs significantly decreased with age (Figure 1f). This decrease in CAMs and coverage outpaced the loss of capillaries (Extended Data Fig. 3a,b), which was previously shown to be an early hallmark of aging in multiple tissues,

118 including central nervous system, lung, kidney, and skin[14,22–26]. To assess if this
119 phenomenon also occurs in humans, we obtained both young and old human patient
120 skin samples. Consistent with our observations in mice, human capillary-associated
121 macrophages also displayed a decline with age. Moreover, CAM decline also outpaced
122 capillary loss with age, suggesting a similar loss in macrophage coverage of the
123 capillary niche (Extended Data Fig. 3c-f). To assess any functional role of CAMs in
124 maintaining capillary blood flow, we performed chemical and genetic ablation of CAMs,
125 via clodronate liposomes and *Cx3cr1-DTR* depletion, respectively, and observed an
126 acute loss in capillary flow (Figure 1 g,h and Extended Data Fig. 4). Collectively, this
127 work highlights an evolutionarily conserved loss in skin capillary-associated
128 macrophages with age, which correlates with impaired homeostatic capillary perfusion.
129

130 **Local CAM recruitment and phagocytosis is required to restore blood flow.**

131 We next aimed to assess the cellular mechanism(s) by which CAMs support
132 capillary blood flow, using a laser-induced blood clotting model to precisely target and
133 stop blood flow in individual capillary segments (Figure 2a, Extended Data Fig. 5a,b and
134 Supplemental Video 6). To assess any macrophage involvement, we tracked the daily
135 displacement of surrounding CAMs to laser-induced clots. These data showed that
136 CAM recruitment to sites of capillary damage as well as RBC engulfment are locally
137 restricted to approximately 80-100μm, and largely occur within the first two days after
138 injury (Figure 2b,c). Under homeostatic conditions, neighboring CAMs were similarly
139 involved locally, taking up RBC debris from naturally occurring capillary clots (Figure
140 2d).

141 Given these findings, we next tested if capillary blood flow was preferentially
142 repaired when at least one resident CAM was in close proximity (<75μm) with the
143 injured capillary segment. The results showed a significant improvement in capillary
144 repair for vessels with an associated macrophage (Extended Data Fig. 5c-e),
145 suggesting that the loss of CAMs could lead to compromised capillary blood flow with
146 age. To rule out an indirect association of capillary repair and CAM proximity, we
147 performed laser-induced ablation of CAMs adjacent to capillary segments immediately
148 prior to inducing capillary clots. Indeed, in regions with CAM ablation within 75μm of the
149 capillary clot, repair was significantly impaired and blood flow was not properly
150 reestablished (Figure 2e,f).

151 Our serial imaging revealed that CAMs at capillary repair sites often contained
152 RBC debris shortly after clot formation. To understand if CAM uptake and clearance of
153 this cellular debris is functionally important for capillary repair, we acutely impaired CAM
154 phagocytosis through inducible cre-dependent knockout of Rac1, a critical component
155 of the phagocytic machinery[27], one week prior to laser-induced clot formation. While
156 there was no significant change in CAM density (Extended Data Fig. 6a,b), we found
157 significant impairment in capillary repair in *Cx3cr1*^{CreER};*Rac1*$^{fl/fl}$ mice compared to
158 *Cx3cr1*^{CreER};*Rac1*$^{fl/+}$ littermate controls (Figure 2g,h), suggesting that Rac1-dependent
159 phagocytic clearance is critical for proper capillary repair and tissue reperfusion.
160 Together, our results support a model in which local CAM recruitment and phagocytic
161 clearance of capillary debris is critical to maintain capillary function. Therefore, as CAM
162 density declines with age, so does capillary perfusion of the tissue (Figure 2i).
163

164 **CAMs do not replenish lost neighbors, resulting in population loss with age**

165 Maintenance of tissue resident macrophage populations in the skin is thought to
166 be mediated through a combination of local proliferation and systemic replacement by
167 blood monocytes[13,28,29]. To understand how CAM density declines with age, we
168 performed single-macrophage lineage tracing, by inducing sparse cre-recombination to
169 label and tracking of individual macrophages over weekly revisits (Extended Data Fig.
170 7a-c). In doing so, we observed discrete behaviors, including macrophage loss and
171 proliferation (Figure 3a). Analysis of weekly rate of CAM loss and division revealed a
172 significant skew toward more CAM loss than division in the first 4 months of age (Figure
173 3b). Consistent with these data, there was a significant decline in the fraction of fate-
174 mapped CAMs over a 20-week time course (Figure 3c). These results demonstrate that
175 the CAMs are insufficiently replenished by local proliferation, which contributes to their
176 progressive decline in this tissue niche.

177 The ability of resident macrophages to locally self-renew has largely been
178 studied through methods of near-total macrophage depletion, which have limited niche-
179 specificity and often generate tissue-wide inflammation[9–11]. To directly interrogate the
180 steps of macrophage self-renewal over time, we tracked both the replacement of
181 individual macrophages after loss and the distribution of sister macrophages after
182 division. First, to track local macrophage replacement after CAM loss, we performed
183 laser-induced ablation of all CAMs within a defined 500μm^2 region. Serial revisits up to
184 two weeks after ablation revealed minimal repopulation from adjacent capillary regions
185 that retained intact CAM populations (Extended Data Fig. 8a and Figure 3d). We found
186 a similar lack in repopulation following partial CAM depletion in *Cx3cr1*^{DTR} mice

187 following low dose diphtheria toxin administration (Figure 3e). To avoid any non-
188 physiological effects from these cell depletion models, we developed a dual fluorescent
189 macrophage reporter mouse, *Cx3cr1-CreERT2; Rosa26-dsRed; Csf1r-EGFP*, allowing
190 for cre-dependent recombination to differentially label a small fraction of macrophages
191 and track their homeostatic replacement. Examination on serial weekly revisits indicated
192 that, as we observed in the depletion models, most capillary niches did not recruit a new
193 macrophage for as long as two weeks following CAM loss (Figure 3f). In contrast,
194 emptied capillary niches were readily replenished with new CAMs when laser-induced
195 macrophage loss was accompanied by laser-induced capillary damage (Figure 3g).
196 Such replenishment was partially CCR2-dependent, suggestive that monocytes may
197 participate in repopulating the capillary niche after injury (Extended Data Fig. 8b-d and
198 Figure 3g). Taken together, these results suggest that CAM loss is not a sufficient
199 trigger to promote neighboring macrophages into the emptied niche.

200 Second, to precisely track sister macrophage migration following cell division, we
201 studied mice with a dual fluorescent nuclear reporter, *Cx3cr1-CreERT2; R26-nTnG*,
202 where we can use low or high doses of tamoxifen to either label individual or all CAMs,
203 respectively (Extended Data Fig. 9a). Compared to the average distance between all
204 neighboring macrophages, sister CAMs remained significantly closer to each other even
205 2 weeks after division (Extended Data Fig. 9b,c). These findings further support the
206 notion that CAM division and loss are not spatiotemporally coupled, which we predict
207 would progressively lead to disorganized patterning and the accumulation of both empty
208 and crowded capillary niches. We tested this prediction by looking at the distribution of
209 neighboring CAMs in both young (2-month old) and old (10-month old) mice. In young

210 mice, the majority of macrophages were within 50μm of each other. In contrast, old mice
211 had a biphasic distribution of macrophage patterning, with most CAMs either within
212 25μm or further than 75μm apart (Extended Data Fig. 9d). These results highlight two
213 distinct cellular features that contribute to reduced CAM coverage with age: 1)
214 insufficient macrophage repopulation following CAM loss, and 2) insufficient distribution
215 of these cells along the capillary niche, which may promote progressive erosion of the
216 vascular bed (Extended Data Fig. 9e).
217

218 **Local CAM replenishment in old mice is sufficient to rejuvenate capillary repair**
219 **and tissue reperfusion**

220 While CAM proliferation was insufficient for maintenance of the population during
221 homeostasis, we asked if extrinsic cues such as broader tissue damage could enhance
222 division rates. We employed large laser-induced wounds in both the epidermal and
223 upper dermal niches (Extended Data Fig. 10a) and found that local CAM proliferation
224 was significantly increased one week following tissue damage in both layers (Extended
225 Data Fig. 10b-e). Given these results we hypothesized that damage-induced CAM
226 proliferation in the aged capillary niche would provide lasting increases in macrophage
227 density. Indeed, broad epidermal damage resulted in a lasting increase in CAMs in
228 damaged regions compared to neighboring control regions (Extended Data Fig. 10f,h).

229 Our results suggest that the capillary-associated macrophage population in old
230 mice can be stably expanded following environmental changes, such as injury.
231 Therefore, we next assessed if increased CAM density, without previous injury, would
232 be sufficient to improve future capillary repair and reperfusion. To this end, we utilized a

233 fusion protein of the canonical macrophage growth factor, CSF1, with the Fc region of
234 porcine IgG, as it has been reported to robustly increase macrophage density in multiple
235 tissues, including skin[30–32]. We performed daily intradermal injections of either CSF1-Fc
236 or PBS in the left or right hind paws, respectively, of the same mice (Figure 4a). There
237 was a significant increase in CAMs in the CSF1-treated paws compared to contralateral
238 PBS controls, which had no significant change from pretreatment (Figure 4b,c).
239 Strikingly, we found that CSF1 treatment was sufficient to improve homeostatic capillary
240 blood flow in old mice, as compared to PBS controls which had significantly more
241 obstructed capillary segments (Figure 4d,e). Utilizing the same aged mice, we next
242 tested if this increase in CAM density would be sufficient to improve capillary repair
243 rates. Following laser-induced clotting, there was a significant improvement in capillary
244 repair and reperfusion in CSF1-treated mice compared to PBS controls (Figure 4 f,g).
245 Consistent with this result, there was also significant improvement in capillary repair and
246 tissue reperfusion in old mice following damage-induced CAM expansion (Extended
247 Data Fig. 10i).
248

249 **Discussion**

250 Macrophage renewal has largely been studied in non-physiological settings, such
251 as through *in vitro* cell culture or severe depletion models that often are accompanied
252 by acute inflammation[9,10,33–35]. Our work clearly demonstrates that homeostatic renewal
253 of resident macrophages is not as finely tuned as has been previously suggested.
254 Specifically, we found that neighboring macrophages do not proliferate or reorganize
255 sufficiently to maintain an optimal population across the skin capillary niche unless they

256 receive additional cues from acute tissue damage or increased growth factor
257 abundance. Interestingly, we confirmed previous findings that show epidermal
258 Langerhans cell density also declines with age, which has been associated with
259 impaired epidermal function[36–39]. This raises the possibility that age-associated loss in
260 macrophage density is a more general phenomenon in populations that rely on local
261 self-renewal.

262 In addition to self-renewal, we also found that CAM recruitment to repair tissue
263 damage was spatially restricted. To our knowledge, the long-term size and stability of
264 resident macrophage territories or niches *in vivo* has not been reported. Our work
265 provides strong evidence that injury-induced macrophage recruitment is restricted to
266 approximately 100μm. In young mice, CAM density is high enough to provide
267 substantial niche/territory overlap between neighbors. However, with declining CAM
268 density with age, we show that a significant fraction of the skin capillary network is no
269 longer within a CAM's territory range. It will be important to understand how this
270 property of CAMs is influenced by other aspects of regional heterogeneity, such as
271 innate immune imprinting[13], to shape local immune responses in tissues.

272 Collectively, this work demonstrates that loss in CAMs: 1) begins within the first
273 few months of life, 2) is progressive throughout life, and 3) is functionally detrimental to
274 vascular function, which has been shown to be a primary driver of age-associated tissue
275 impairments[15,40]. Furthermore, this work provides a novel platform to investigate age-
276 associated deviations in tissue homeostasis at the single-cell level in a living mammal.
277
278

References

1. Nobs, S. P. & Kopf, M. Tissue-resident macrophages: guardians of organ homeostasis. *Trends Immunol* **42**, 495–507 (2021).

2. Minutti, C. M., Knipper, J. A., Allen, J. E. & Zaiss, D. Tissue-specific contribution of macrophages to wound healing. *Semin Cell Dev Biol* **61**, 3–11 (2017).

3. Vannella, K. M. & Wynn, T. A. Mechanisms of Organ Injury and Repair by Macrophages. *Annual Review of Physiology* **79**, (2016).

4. Chakarov, S. *et al.* Two distinct interstitial macrophage populations coexist across tissues in specific subtissular niches. *Science* **363**, eaau0964 (2019).

5. Wu, Y. & Hirschi, K. K. Tissue-Resident Macrophage Development and Function. *Frontiers Cell Dev Biology* **8**, 617879 (2021).

6. Beek, A. A. van, Bossche, J. den, Mastroberardino, P. G., Winther, M. de & Leenen, P. Metabolic Alterations in Aging Macrophages: Ingredients for Inflammaging? *Trends Immunol* (2019) doi:10.1016/j.it.2018.12.007.

7. Franceschi, C., Garagnani, P., Vitale, G., Capri, M. & Salvioli, S. Inflammaging and 'Garb-aging.' *Trends Endocrinol Metabolism* **28**, 199–212 (2017).

8. Mass, E., Nimmerjahn, F., Kierdorf, K. & Schlitzer, A. Tissue-specific macrophages: how they develop and choreograph tissue biology. *Nat. Rev. Immunol.* 1–17 (2023) doi:10.1038/s41577-023-00848-y.

9. Bruttger, J. *et al.* Genetic Cell Ablation Reveals Clusters of Local Self-Renewing Microglia in the Mammalian Central Nervous System. *Immunity* **43**, 92–106 (2015).

10. Sakai, M. *et al.* Liver-Derived Signals Sequentially Reprogram Myeloid Enhancers to Initiate and Maintain Kupffer Cell Identity. *Immunity* **51**, 655-670.e8 (2019).

11. Hashimoto, D. *et al.* Tissue-Resident Macrophages Self-Maintain Locally throughout Adult Life with Minimal Contribution from Circulating Monocytes. *Immunity* **38**, 792–804 (2013).

12. Okabe, Y. & Medzhitov, R. Tissue biology perspective on macrophages. *Nature Immunology* **17**, 9–17 (2016).

13. Guilliams, M., Thierry, G. R., Bonnardel, J. & Bajenoff, M. Establishment and Maintenance of the Macrophage Niche. *Immunity* **52**, 434–451 (2020).

310 14. Fukada, K. & Kajiya, K. Age-related structural alterations of skeletal muscles and
311 associated capillaries. *Angiogenesis* **23**, 79–82 (2020).

312 15. Grunewald, M. *et al.* Counteracting age-related VEGF signaling insufficiency
313 promotes healthy aging and extends life span. *Science* **373**, eabc8479 (2021).

314 16. Pluvinage, J. V. & Wyss-Coray, T. Systemic factors as mediators of brain
315 homeostasis, ageing and neurodegeneration. *Nat Rev Neurosci* **21**, 93–102 (2020).

316 17. Shaw, A. C., Goldstein, D. R. & Montgomery, R. R. Age-dependent dysregulation of
317 innate immunity. *Nature reviews. Immunology* (2013) doi:10.1038/nri3547.

318 18. Pineda, C. M. *et al.* Intravital imaging of hair follicle regeneration in the mouse.
319 *Nature protocols* **10**, 1116–30 (2015).

320 19. Mesa, K. R. *et al.* Homeostatic Epidermal Stem Cell Self-Renewal Is Driven by
321 Local Differentiation. *Cell Stem Cell* (2018) doi:10.1016/j.stem.2018.09.005.

322 20. Dietzel, S. *et al.* Label-Free Determination of Hemodynamic Parameters in the
323 Microcirculaton with Third Harmonic Generation Microscopy. *PLoS ONE* **9**, e99615
324 (2014).

325 21. Saytashev, I. *et al.* Multiphoton excited hemoglobin fluorescence and third harmonic
326 generation for non-invasive microscopy of stored blood. *Biomedical Optics Express* **7**,
327 3449 (2016).

328 22. Bentov, I. & Reed, M. J. The effect of aging on the cutaneous microvasculature.
329 *Microvasc Res* **100**, 25–31 (2015).

330 23. Smith, L. Histopathologic characteristics and ultrastructure of aging skin. *Cutis* **43**,
331 414–24 (1989).

332 24. Li, L. *et al.* Age-Related Changes of the Cutaneous Microcirculation in vivo.
333 *Gerontology* **52**, 142–153 (2006).

334 25. Reeson, P., Choi, K. & Brown, C. E. VEGF signaling regulates the fate of obstructed
335 capillaries in mouse cortex. *eLife* **7**, e33670 (2018).

336 26. Das, A. *et al.* Impairment of an Endothelial NAD+-H2S Signaling Network Is a
337 Reversible Cause of Vascular Aging. *Cell* **173**, 74-89.e20 (2018).

338 27. Cox, D. *et al.* Requirements for Both Rac1 and Cdc42 in Membrane Ruffling and
339 Phagocytosis in Leukocytes. *J Exp Medicine* **186**, 1487–1494 (1997).

340 28. Perdiguero, E. & Geissmann, F. The development and maintenance of resident
341 macrophages. *Nat Immunol* **17**, 2–8 (2015).

29. Blériot, C., Chakarov, S. & Ginhoux, F. Determinants of Resident Tissue Macrophage Identity and Function. *Immunity* **52**, 957–970 (2020).

30. Alfituri, O. A., Mararo, E. M., Steketee, P. C., Morrison, L. J. & Mabbott, N. A. Dermal bacterial LPS-stimulation reduces susceptibility to intradermal Trypanosoma brucei infection. *Sci Rep-uk* **11**, 9856 (2021).

31. Gow, D. J. *et al.* Characterisation of a Novel Fc Conjugate of Macrophage Colony-stimulating Factor. *Mol Ther* **22**, 1580–1592 (2014).

32. Keshvari, S. *et al.* Therapeutic potential of macrophage colony-stimulating factor in chronic liver disease. *Dis Model Mech* **15**, dmm049387 (2022).

33. Zhou, X. *et al.* Circuit Design Features of a Stable Two-Cell System. *Cell* **172**, 744-757.e17 (2018).

34. Nicolás-Ávila, J. A. *et al.* A Network of Macrophages Supports Mitochondrial Homeostasis in the Heart. *Cell* **183**, 94-109.e23 (2020).

35. Ferrer, I. R. *et al.* A wave of monocytes is recruited to replenish the long-term Langerhans cell network after immune injury. *Sci Immunol* **4**, eaax8704 (2019).

36. Gilchrest, B. A., Murphy, G. F. & Soter, N. A. Effect of Chronologic Aging and Ultraviolet Irradiation on Langerhans Cells in Human Epidermis. *J Invest Dermatol* **79**, 85–88 (1982).

37. Cruchley, A. T. *et al.* Langerhans cell density in normal human oral mucosa and skin: relationship to age, smoking and alcohol consumption. *J Oral Pathol Med* **23**, 55–59 (1994).

38. Hasegawa, T. *et al.* Reduction in human epidermal Langerhans cells with age is associated with decline in CXCL14-mediated recruitment of CD14+ monocytes. *J Invest Dermatol* (2019) doi:10.1016/j.jid.2019.11.017.

39. Fenske, N. A. & Lober, C. W. Structural and functional changes of normal aging skin. *J Am Acad Dermatol* **15**, 571–585 (1986).

40. Cai, C. *et al.* Impaired dynamics of precapillary sphincters and pericytes at first-order capillaries predict reduced neurovascular function in the aging mouse brain. *Nat Aging* **3**, 173–184 (2023).

Acknowledgements

We thank members of the Littman lab for valuable discussion and critical reading of the manuscript. We thank Michael Cammer from the NYU Microscopy Core for valuable discussion, training and technical support. The Microscopy Core is partially supported by NYU Cancer Center Support Grant NIH/NCI P30CA016087 at the Laura and Isaac Perlmutter Cancer Center, S10 RR023704-01A1 and NIH S10 ODO019974-01A1. This work was supported by a Jane Coffin Childs Fund fellowship (K.R.M.), Kirschstein-NRSA training grant T32AR64184 (K.R.M.), Kirschstein-NRSA individual postdoctoral fellowship F32AG071336 (K.R.M.), a Charles H. Revson Senior Fellowship in Biomedical Science (K.R.M.), the Helen and Martin Kimmel Center for Biology and Medicine (D.R.L.), NIH grant R01AI158687 (D.R.L.), and the Howard Hughes Medical Institute (D.R.L.).

Author Contributions

K.R.M. and D.R.L. designed the study and analyzed the data; K.R.M. and K.A.O. performed mouse experiments. K.R.M. performed intravital multiphoton imaging. C.N. and S.P.S. provided human biological samples and related quantitative analysis. K.R.M. and D.R.L. wrote the manuscript, with input from the other authors. D.R.L. supervised the research.

398 **Figures**

Figure 1

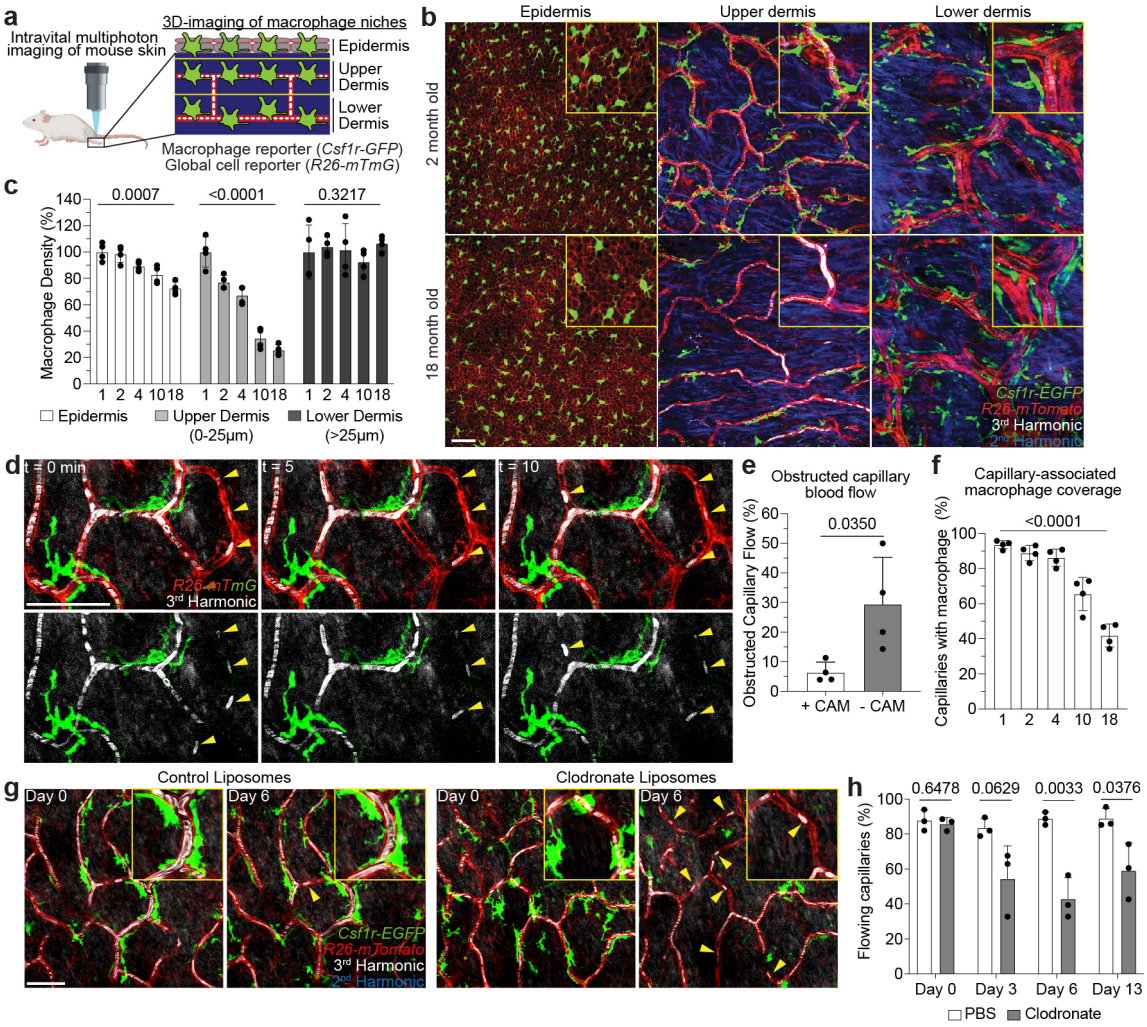

399

400 **Figure 1 –Niche-specific macrophage loss with age correlates with impaired skin**

401 **capillary blood flow. a,** Schematic of intravital imaging of resident macrophage

402 populations in mouse skin, indicating epidermal and dermal populations, using the

403 macrophage reporter, *Csf1r-EGFP,* in combination with an *Actb*-driven universal

404 tdTomato reporter, *R26-mTmG*. **b,** Representative optical sections of distinct resident

405 macrophage populations in young (2-month-old) and old (18-month-old) mice. **c,**

406 Quantification of niche-specific macrophage density change in 1, 2, 4, 10, and 18 month

407 old mice (n = 4 mice in each age group; two 500μm^2 regions per mouse; macrophage

density in each skin niche was compared across age groups by one-way ANOVA; mean ± SD). **d,** Skin resident macrophage labeling using *Cx3cr1-CreERT2;R26-mTmG* mice was performed following a single high-dose intraperitoneal injection of tamoxifen (2mg) in 1 month old mice. Single optical sections at successive time points 5 min apart showing red blood cell (RBC) flow (white) in capillaries (red) with or without nearby CAMs (green). Yellow arrowheads indicate obstructed RBC capillary flow. **e,** Quantification of obstructed capillary flow as measured by stalled RBCs as described in Extended Data Figure 2 (n = 226 CAM+ capillary segments, n = 27 CAM- capillary segments; n = 4 mice; obstructed capillary flow (CAM+ vs CAM-) was compared by paired Student's t test; mean ± SD). **f,** Percentage of capillary segments with at least one associated macrophage (n = 4 mice in each age group; two 500μm^2 regions per mouse; macrophage association with capillary segments was compared across age groups by one-way ANOVA; mean ± SD). **g,** Representative images demonstrate macrophage depletion following intradermal injections of clodronate-liposomes every 3 days. Repeated intravital imaging of the vascular niche was performed to visualize macrophages (*Csf1r-GFP*), capillaries (*R26-mTmG*) and RBC flow (Third Harmonic). **h,** Percentage of capillaries with blood flow following macrophage depletion (n = 194 capillary segments in clodronate group, n = 199 capillary segments in PBS group; 3 mice in each group; capillary flow (clodronate vs PBS) was compared by unpaired Student's t test; mean ± SD). Scale bar, 50 μm.

Figure 2

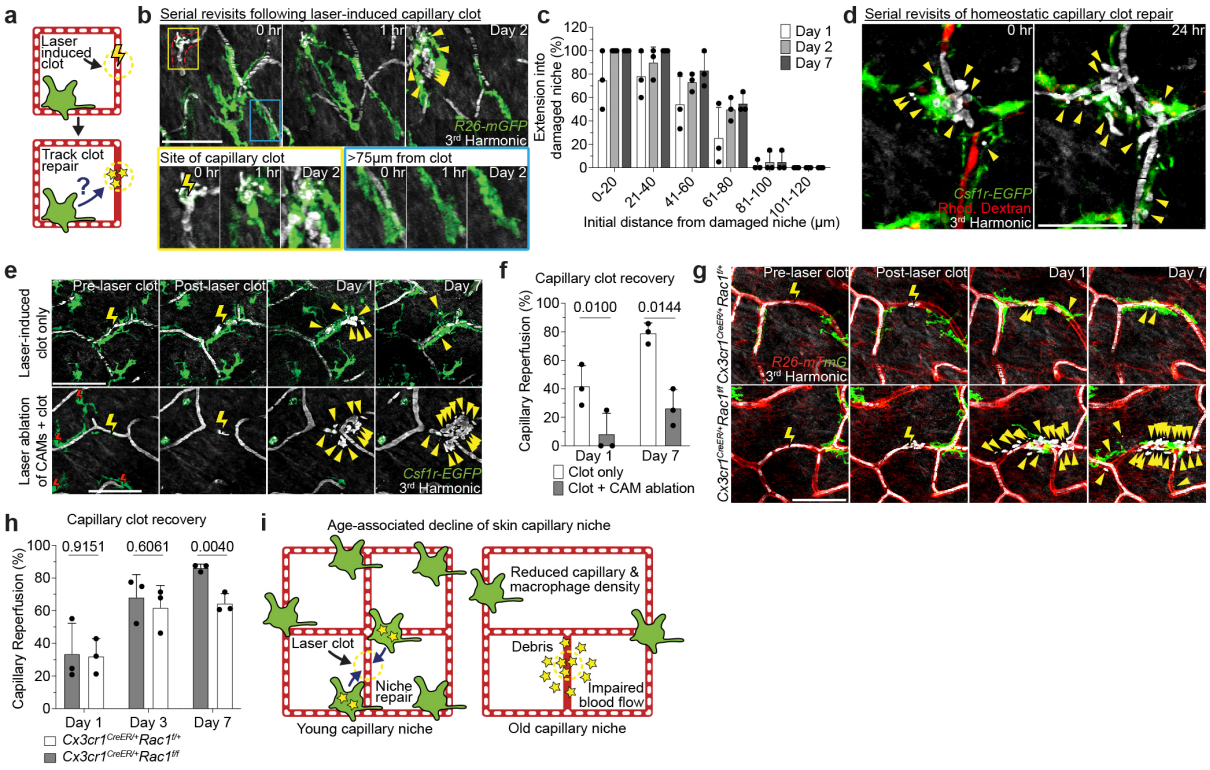

Figure 2 – Local CAM recruitment and phagocytosis are required to restore impaired blood flow. a, Scheme of laser-induced capillary clot experiment. **b,** Sequential revisits of damaged capillary segment (red dashed lines) after laser-induced clot formation in *Cx3cr1-CreERT2;R26-mTmG* mice. Yellow lightning bolt indicates site of laser-induced capillary clot. Yellow arrowheads indicate extra-luminal vascular debris. **c,** Quantification of capillary-associated macrophage extension toward damaged niche at Day 1, 2 and 7 after laser-induced clotting (n = 50 CAMs, in 3 mice; mean ± SD). **d,** Sequential revisits of naturally forming capillary clots in *Csf1r-EGFP* mice. Simultaneous visualization of blood flow during clot repair via third harmonic generation (white) from red blood cells (RBC) and intravenous rhodamine dextran (RhDex) (red). **e,** Sequential revisits of damaged capillary niche after laser-induced CAM ablation and clot formation in *Csf1r-EGFP* mice. Macrophage laser ablation (red lightning bolt) and capillary clot

444 formation (yellow lightning bolt) were both performed at 940nm for 1s. **f,** Quantification
445 of capillary reperfusion at Day 1 and 7 after laser-induced clotting and macrophage
446 ablation (n = 19 capillary clots in CAM ablated regions, n = 16 capillary clots in control
447 regions; 3 mice in total; capillary reperfusion (CAM ablated vs control) was compared by
448 paired Student's t test; mean ± SD). **g,** Sequential revisits of damaged capillary niche
449 after laser-induced clot formation in *Cx3cr1*^{CreER};*Rac1*$^{fl/fl}$ and *Cx3cr1*^{CreER};*Rac1*$^{fl/+}$ mice.
450 CAMs (green), capillaries (red), RBC (white). **h,** Quantification of capillary reperfusion at
451 Day 1, 3 and 7 after laser-induced clotting (n = 67 clots in *Rac1*$^{fl/+}$ group; n = 82 clots in
452 *Rac1*$^{fl/fl}$ group; n = 3 mice in each group; capillary reperfusion (*Rac1*$^{fl/+}$ vs *Rac1*$^{fl/fl}$) was
453 compared by unpaired Student's t test; mean ± SD). **i,** Scheme of age-associated
454 decline of skin capillary niche. Capillary-associated macrophage density declines with
455 age, which predisposes aged capillaries to impaired repair and sustained tissue
456 perfusion. Scale bar, 50μm.
457
458
459
460
461
462
463
464
465
466

Figure 3

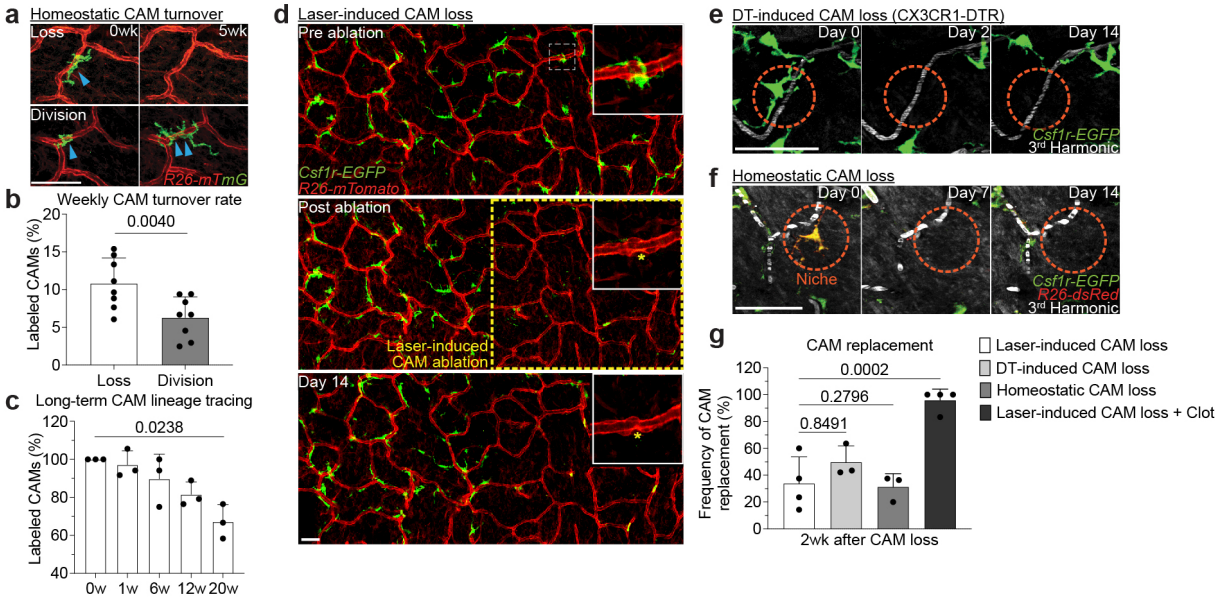

Figure 3 – Capillary-associated macrophages do not replenish lost neighbors, resulting in population loss with age. a, Representative revisits of single macrophage lineage tracing (blue arrowhead) in *Cx3cr1-CreERT2*; *R26-mTmG* mice. Weekly revisits were performed during homeostatic conditions for 20 weeks following a single low-dose intraperitoneal injection of tamoxifen (50µg). **b,c,** Quantification of (b) weekly rate of CAM loss and division (n = 262 CAMs; 8 mice in total; CAM turnover rates (CAM loss vs division) was compared by paired Student's t test; mean ± SD) and of (c) maintenance of the labeled CAM population over 20wk lineage tracing (n = 59 CAMs; 3 mice in total; number of fluorescently-labeled CAMs was compared across each time point in the same mice by one-way repeated measures ANOVA with Geisser-Greenhouse correction; mean ± SD). **d,** Representative revisits of CAM replacement after laser-induced CAM ablation in *Csf1r-EGFP;R26-mTmG* mice. Macrophage laser ablations (yellow asterisk) were performed in a 500µm^2 region (yellow dashed line square), **e,** Representative revisits of CAM replacement after a single intraperitoneal injection

482 diphtheria toxin (10ng/g body weight in PBS) in *Cx3cr1-DTR* mice. **f,** Representative
483 revisits of single lineage-tracked macrophages in *Cx3cr1-CreERT2*; *R26-dsRed*; *Csf1r-*
484 *EGFP* mice. Weekly revisits were performed during homeostatic conditions for 2 weeks
485 following a single low-dose intraperitoneal injection of tamoxifen (50µg). **g,**
486 Quantification of replenishment rate of empty CAM niche under laser-induced loss (n =
487 44 CAMs; 4 mice in total), DT-induced loss (n = 53 CAMs; 3 mice in total), homeostatic
488 loss (n = 29 CAMs; 3 mice in total), or laser-induced CAM loss with capillary clot (n = 25
489 CAMs; 4 mice in total). Frequency of CAM replacement after forced and homeostatic
490 CAM loss were compared by unpaired Student's t test; mean ± SD. Scale bar, 50µm.
491
492
493
494
495
496
497
498
499
500
501
502
503
504

Figure 4

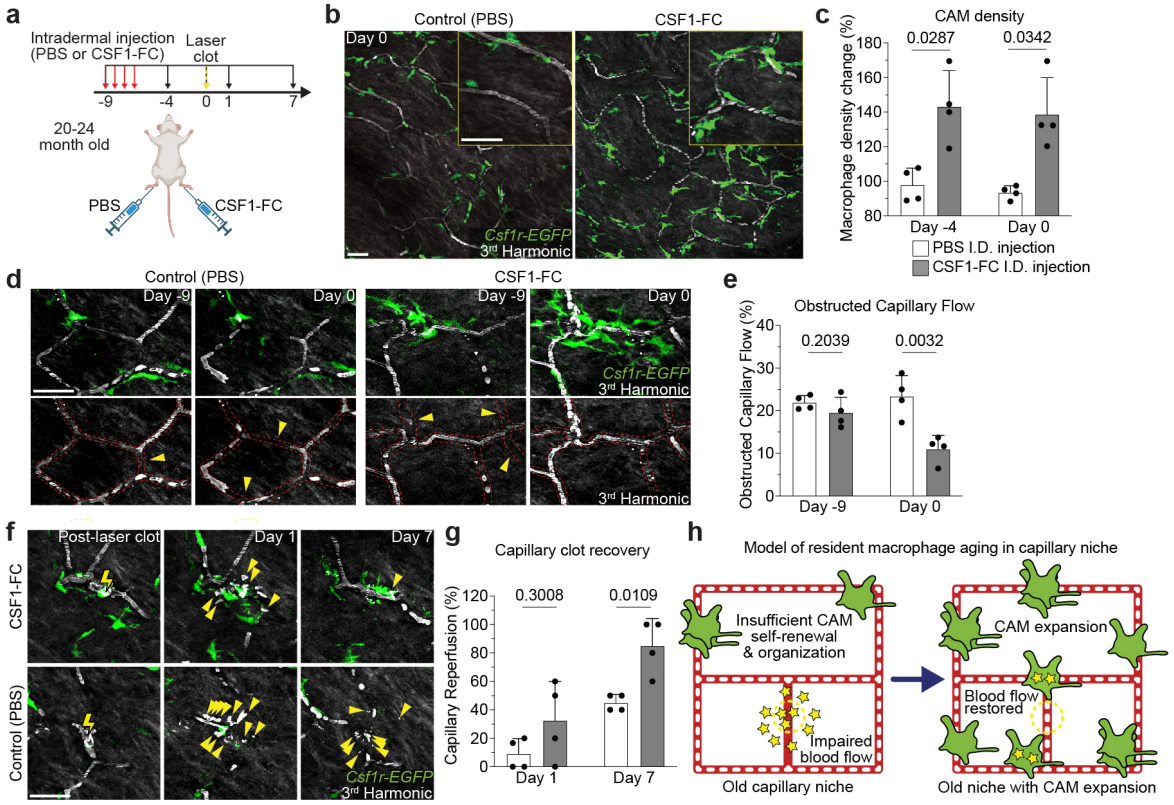

Figure 4 –Local CAM replenishment in old mice is sufficient to rejuvenate capillary repair and tissue reperfusion. a, Scheme of CSF1-induced rejuvenation of aged capillary niche. **b,** Representative images of CAM density in *Csf1r-EGFP* mice nine days following daily intradermal injections (4 days) of CSF1-Fc (porcine CSF1 and IgG1a Fc region fusion protein) and PBS in contralateral hind paws of 20-24 month old mice. **c,** Quantification of CAM density following CSF1-Fc or PBS treatment (n = 4 mice in total; two 500μm^2 regions of each treatment condition per mouse; Percentage of CAM density change from Day -9 (CSF1-Fc vs PBS) was compared for Day -4 and Day 0 time points by paired Student's t test; mean ± SD). **d,** Representative images of capillary (red dashed lines) blood flow in *Csf1r-EGFP* mice nine days following daily intradermal injections of CSF1-Fc and PBS in contralateral hind paws of 20-24 month

old mice. Yellow arrowheads indicate obstructed RBC capillary flow. **e,** Quantification of obstructed capillary blood flow following CSF1-Fc or PBS treatment (n = 214 capillary segments in CSF1-Fc treated regions, n = 214 capillary segments in PBS treated regions; n = 4 mice in total; obstructed capillary flow (CSF1-Fc vs PBS) was compared for Day -9 and Day 0 time points by paired Student's t test; mean ± SD). **f,** Sequential revisits of damaged capillary niche after laser-induced clot formation (yellow lightning bolt) in *Csf1r-EGFP* mice. Yellow arrowheads indicate extra-luminal vascular debris. **g,** Quantification of capillary reperfusion at Day 1 and 7 after laser-induced clotting (n = 18 clots in CSF1-Fc group; n = 20 clots in PBS group; n = 4 mice in total; capillary reperfusion (CSF1-Fc vs PBS) was compared by paired Student's t test; mean ± SD). **h,** Working model of resident macrophage aging in the skin capillary niche. Age-associated impairment in capillary repair can be rejuvenated following local expansion of resident macrophage population. Scale bar, 50μm.

540 **Methods**

541

542 **Mice**

543 Mice were bred and maintained in the Alexandria Center for the Life Sciences animal
544 facility of the New York University School of Medicine, in specific pathogen-free
545 conditions. Albino B6 (B6(Cg)-*Tyr*$^{c-2J}$/J, Jax 000058), Csf1r^{EGFP} (B6.Cg-Tg(Csf1r-
546 EGFP)1Hume/J, Jax 018549), Ccr2^{RFP} (B6.129(Cg)-Ccr2tm2.1Ifc/J, Jax 017586),
547 R26^{mTmG} (B6.129(Cg)-Gt(ROSA)26Sortm4(ACTB-tdTomato,-EGFP)Luo/J, Jax 007676),
548 R26^{nTnG} (B6N.129S6-Gt(ROSA)26Sortm1(CAG-tdTomato*,-EGFP*)Ees/J, Jax 023537),
549 LysM^{Cre} (B6.129P2-Lyz2tm1(cre)Ifo/J, Jax 004781), Rac1$^{f/f}$ (Rac1tm1Djk/J, Jax 005550)
550 mice were purchased from Jackson Laboratories. *R26*^{dsRed} mice were described
551 previously (Luche et al., 2007) and were obtained from the laboratory of Dr. Gordon
552 Fishell. *Cx3cr1*^{CreER}, *Cx3cr1*^{GFP}*, and Cx3cr1*^{DTR} were generated in our laboratory and
553 have been described (3 ref). Cre-induction for the lineage tracing or total CAM labeling
554 experiments was induced with a single intraperitoneal injection of Tamoxifen (Sigma-
555 Aldrich; T5648) (100µg or 4mg in corn oil, respectively) in 1 month old mice. *Rac1*$^{f/f}$
556 recombination was induced with two intraperitoneal injections of Tamoxifen (2mg in corn
557 oil) 48hrs apart in 1 month old mice. All imaging and experimental manipulation are
558 performed on non-hairy mouse plantar (hind paw) skin. Preparation of skin for intravital
559 imaging are performed as described below. Briefly, mice are anesthetized with
560 intraperitoneal injection of ketamine/xylazine (15 mg/ml and 1 mg/ml, respectively in
561 PBS). After imaging, mice are returned to their housing facility. For subsequent revisits,
562 the same mice are processed again with injectable anesthesia. The plantar epidermal

563 regions are briefly cleaned with PBS pH 7.2, mounted on a custom-made stage and a
564 glass coverslip are placed directly against the skin. Anesthesia is maintained throughout
565 the course of the experiment with vaporized isoflurane delivered by a nose cone. Mice
566 from experimental and control groups were randomly selected for live imaging
567 experiments. No blinding was done. All lineage tracing and ablation experiments were
568 repeated in at least three different mice. All animal procedures were performed in
569 accordance with protocols approved by the Institutional Animal Care and Usage
570 Committee of New York University School of Medicine.

571 ***In vivo* imaging and laser ablation**

572 Image stacks were acquired with an Olympus multiphoton FVMPE-RS system equipped
573 with both InSight X3 and Mai Tai Deepsee (Spectra-Physics) tunable Ti:Sapphire
574 lasers, using Fluoview software. For collection of serial optical sections, a laser beam
575 (940nm for GFP/tdTomato/dsRed/RFP/Rhodamine/Second Harmonic Generation and
576 1300nm for Third Harmonic Generation, respectively) was focused through a water
577 immersion lens (N.A. 1.05; Olympus) and scanned with a field of view of 0.5mm^2, at
578 600 Hz. Z-stacks were acquired in 1-2μm steps for a ~50-100μm range, covering the
579 epidermis and dermis. Capillary blood flow was visualized in some experiments through
580 intravenous injection with 18 mg/kg of dextran-rhodamine 70 kD (Sigma-Aldrich;
581 R9379). Cell tracking analysis was performed by re-visiting the same area of the dermis
582 in separate imaging experiments through using inherent landmarks of the skin to
583 navigate back to the original region, including the distinct organization of the superficial
584 vasculature networks. Cells that were unambiguously separated (by at least 250μm)
585 from another were sampled to ensure the identity of individual lineages. For time-lapse

586 recordings, serial optical sections were obtained between 5-10 minute intervals,
587 depending on the experimental setup. Laser-induced cell ablation, capillary clot, or
588 tissue damage was carried out with the same optics as used for acquisition. An 940nm
589 laser beam was used to scan the target area (1-500μm^2) and ablation was achieved
590 using 50-70% laser power for ~1sec. Ablation parameters were adjusted according to
591 the depth of the target (10-50μm). Mice from experimental and control groups were
592 randomly selected for live imaging experiments. No blinding was done. All lineage
593 tracing and ablation experiments were repeated in at least three different mice.
594

595 **Drug treatments**

596 To induce macrophage depletion, mice received intradermal injections of either
597 Clodronate-liposomes or PBS-liposomes (stock concentration 5mg/ml; Liposoma; CP-
598 005-005) (5μl per paw) every 3 days. Depending on experimental details, Cx3cr1^{DTR}
599 mice received either intraperitoneal (IP) injection of diphtheria toxin (Sigma-Aldrich;
600 D0564) every other day at 25ng/g body weight in PBS or a single low dose IP injection
601 at 10ng/g body weight in PBS. To induce macrophage expansion, mice receive daily
602 intradermal injections of CSF1-FC (Bio-Rad; PPP031) or PBS in contralateral hind paws
603 (5μl per paw) for 4 days.
604

605 **Human skin samples**

606 Written informed consent was obtained for postmortem examination from next of kin for
607 10 patients. Clinical information and laboratory data were obtained from the electronic
608 medical record. Skin samples were obtained from the anterolateral chest and fixed in

609 10% formalin for at least 24h prior to processing. Slides were stained with hematoxylin
610 and eosin, CD68 (Clone 514H12) and ERG (Clone EPR3864). Macrophages and
611 capillaries were identified using a combination of morphology, CD68 and ERG staining.
612 Counting was performed on at least eight high-power fields (40x) within 100um of the
613 epidermis.
614

615 **Image Analysis**

616 Raw image stacks were imported into Fiji (NIH, USA) or Imaris software (Bitplane/Perkin
617 Elmer) for further analysis. Provided images and supplementary videos are typically
618 presented as a maximal projection of 4-8µm optical sections. For visualizing individual
619 labeled cells expressing the dsRed or tdTomato Cre reporters, the brightness and
620 contrast were adjusted accordingly for the green (GFP) and red (dsRed/tdTomato)
621 channels and composite serial image sequences were assembled as previously
622 described. Images were obtained as large tiled image stacks at roughly the same
623 positions and then manually aligned over the experimental time course in Imaris
624 (Bitplane/Perkin Elmer) by using data from all channels.
625

626 **Statistical Analysis**

627 Data are expressed as mean ± SD. An unpaired Student's *t*-test was used to analyze
628 data sets with two groups. One-way ANOVA was used to analyze data sets with three
629 or more groups. $p < 0.05$ to $p < 0.0001$ indicated a significant difference. Statistical
630 calculations were performed using the Prism software package (GraphPad, USA).
631

632 **Extended Data Figure Legends**

Extended Data Figure 1

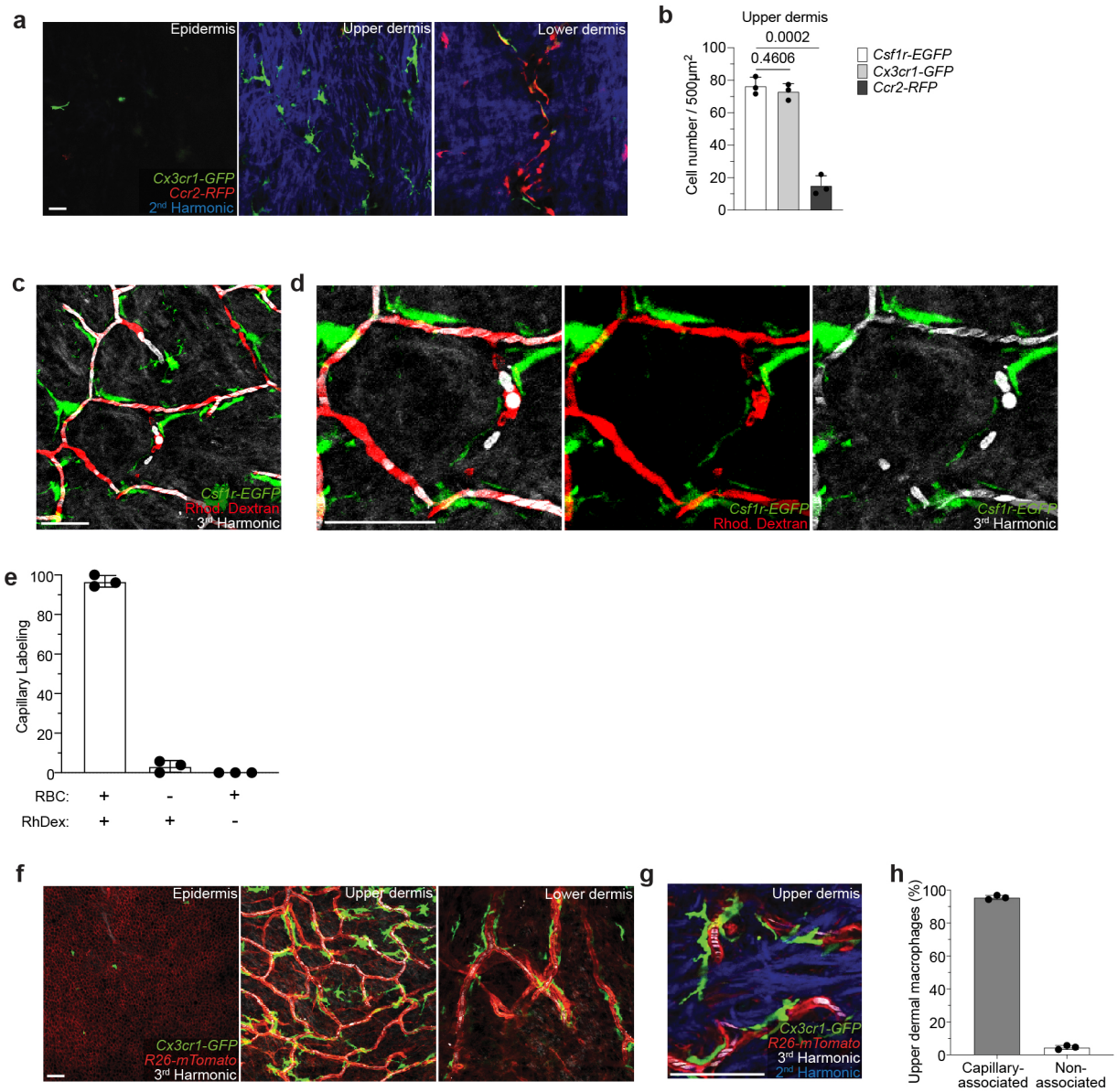

633

634 **Extended Data Figure 1. CX3C-chemokine receptor 1 (CX3CR1) expression in the**

635 **upper dermis defines a resident population of capillary-associated macrophages**

636 **(CAMs).** a) Representative images of cells expressing *Ccr2-RFP*, *Csf1r-EGFP*, or

637 *Cx3cr1-GFP* in the epidermis, upper dermis, and lower dermis of 1 month old mice. b)

638 Quantifications of cells expressing *Csf1r-EGFP*, *Cx3cr1-GFP, or Ccr2-RFP*, in the upper

639 dermis (n = 3 mice in each group; two 500μm^2 regions per mouse; Cell number (*Csf1r-*
640 *EGFP* vs *Cx3cr1-GFP; Csf1r-EGFP* vs *Ccr2-RFP*) was compared by unpaired Student's
641 t test; mean ± SD). c-d) Simultaneous visualization of blood flow through the superficial
642 capillary plexus via third harmonic generation (white) from red blood cells (RBC) and
643 intravenous rhodamine dextran (RhDex) (red). e) Quantifications of RBC and RhDex
644 labeling of the upper dermal superficial capillary plexus (n = 3 mice in total; four 500μm^2
645 regions per mouse; mean ± SD). f) Visualization of CX3CR1-expressing cells in all skin
646 layers: epidermis, upper dermis, and lower dermis (*Cx3cr1-GFP;R26-mTmG*) was
647 performed during homeostatic conditions. g) Representative image of labeled upper
648 dermal macrophages in contact with capillary superficial plexus (red) in 1 month old
649 mice. h) Quantifications reveal most upper dermal macrophages are capillary-
650 associated macrophages (CAMs) (n = 3 mice in total; three 500μm^2 regions per mouse;
651 mean ± SD) . Scale bar, 50 μm.
652
653
654
655
656
657
658
659
660

Extended Data Figure 2

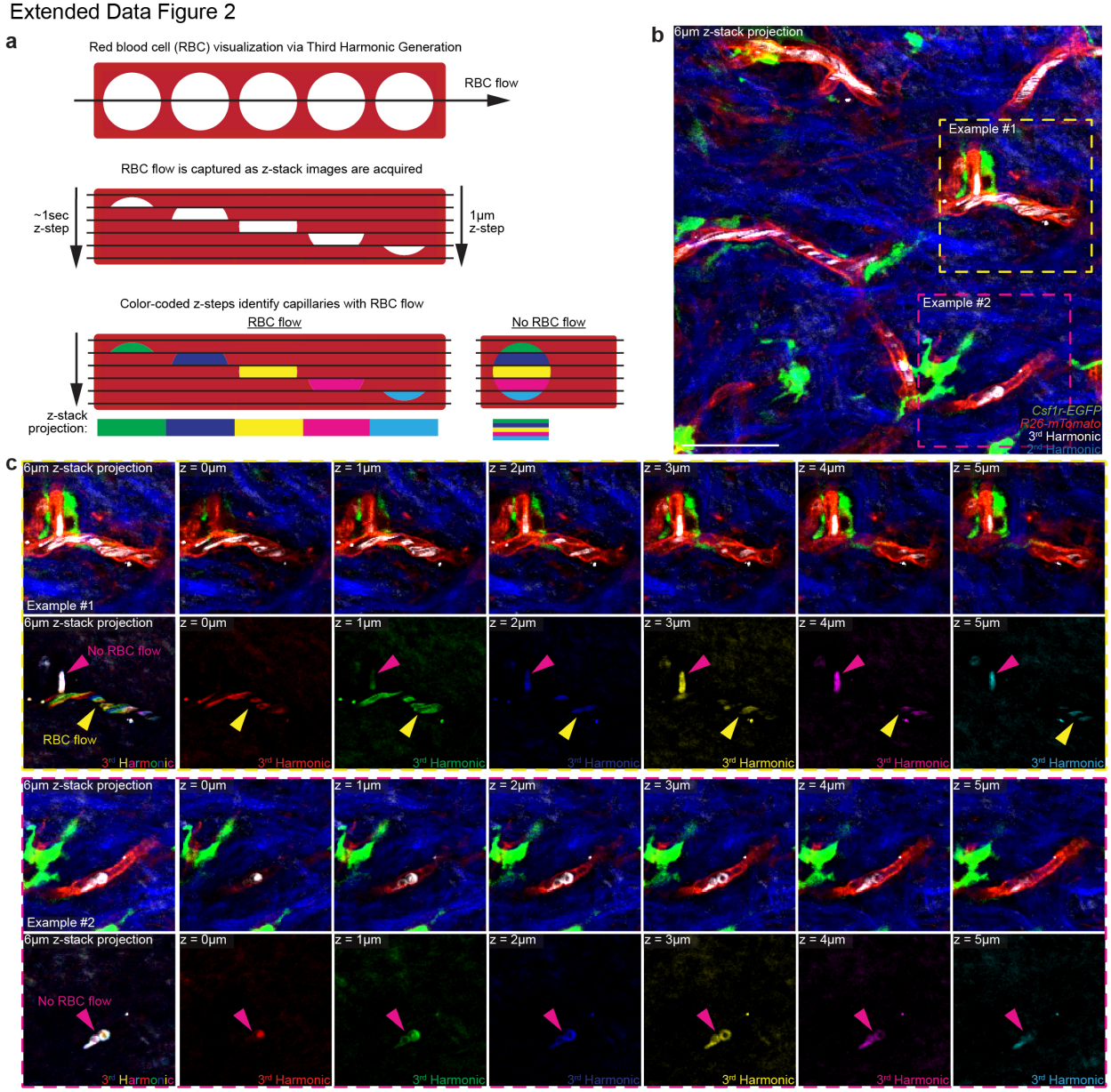

Extended Data Figure 2. Label-free *in vivo* visualization of capillary blood flow via third harmonic effect generated by red blood cells. a, Scheme of red blood cell (RBC) flow through a segment of the superficial skin capillary network. During three-dimensional image acquisition, flowing red blood cells are captured at different x,y positions for each z-section along the capillary segment. Pseudocoloring each z-step through a capillary segment distinguishes flowing RBCs as a multicolor patchwork or

668 rainbow-effect and leaves obstructed/non-flowing RBCs as white (full overlap of all
669 colors). **b,** Representative image of RBC visualization in the upper dermis in *Csf1r-*
670 *EGFP; R26-mTmG* mice. **c,** Representative optical z-sections through upper dermal
671 capillaries. Third harmonic signal is pseudocolored differently for each z-step to
672 visualize RBC movement along the capillary segments during image acquisition. Scale
673 50μm.
674
675
676
677
678
679
680
681
682
683
684
685
686
687
688
689
690

Extended Data Figure 3

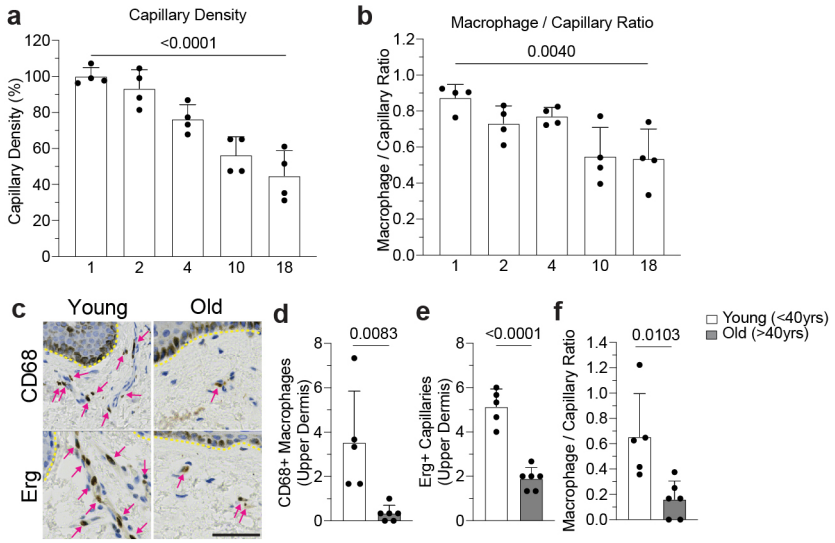

Extended Data Figure 3. Capillary and associated macrophage loss in mice and humans. a,b Quantification of capillary niche age-associated changes, (a) Capillary density and (b) CAM / Capillary segment ratio (n = 4 mice in each age group; two 500μm^2 regions per mouse; comparison across age groups was by one-way ANOVA; mean ± SD). **c,** Representative immunohistochemistry of CD68+ macrophage and Erg+ capillary density in the upper dermis of both young (<40y) and old (>40y) human samples. **d-f,** Quantification of capillary niche age-associated changes: (d) CD68+ macrophage density, (e) Erg+ capillary density, (f) Upper dermal macrophage / Capillary endothelium ratio (n = 5 patient samples in each group; three imaging regions per sample; Comparison by unpaired Student's t test; mean ± SD). Scale bar, 50μm.

Extended Data Figure 4

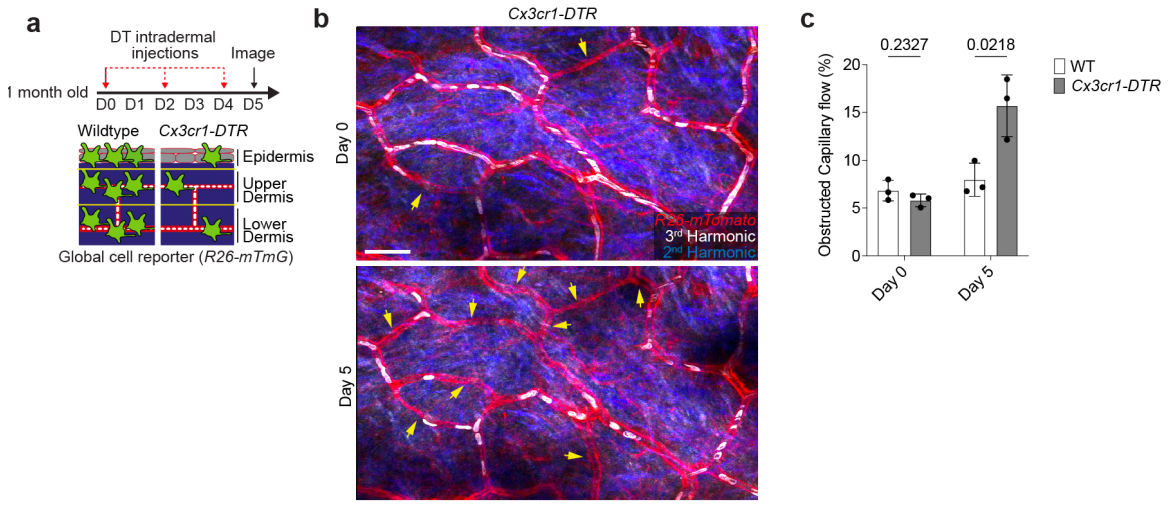

Extended Data Figure 4. Impaired skin capillary blood flow following acute macrophage depletion. a, Scheme of long-term capillary blood flow tracking following intraperitoneal injection every other day with diphtheria toxin (DT) (25ng/g body weight in PBS) in both *Cx3cr1-DTR*; *R26-mTmG* and WT control (*R26-mTmG*) mice. **b,** Representative revisits of the same capillary network to visualize capillaries (*R26-mTmG*) and RBC flow (Third Harmonic). **c,** Quantifications reveal a significant reduction in the percentage of capillaries with blood flow following DT-induced cell depletion (n = 647 capillary segments in WT control regions, n = 695 capillary segments in *Cx3cr1-DTR* regions; n = 3 mice in each group; obstructed capillary flow (WT vs *Cx3cr1-DTR*) was compared for Day 0 and Day 5 time points by unpaired Student's t test; mean ± SD). Scale bar, 50 μm.

Extended Data Figure 5

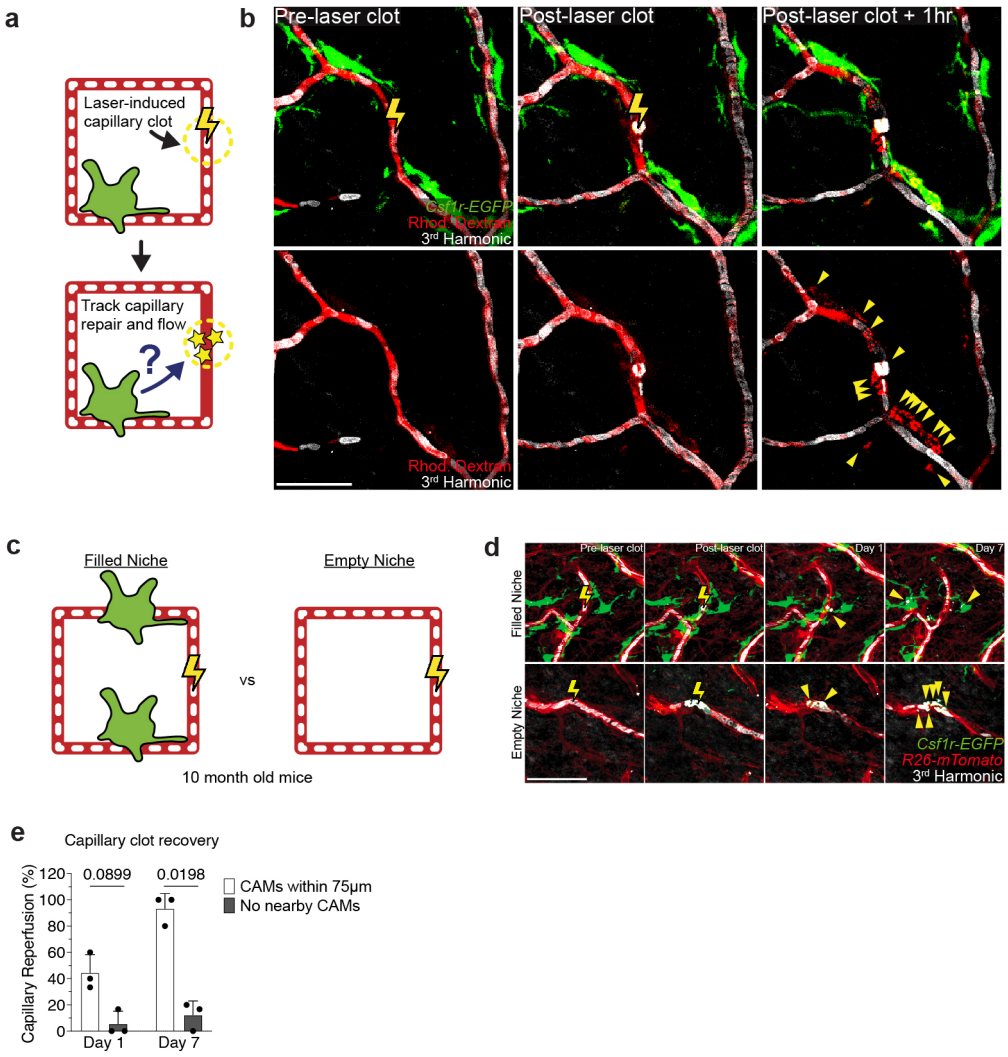

Extended Data Figure 5. Laser-induced model of acute capillary clot formation and repair. a, Scheme of laser-induced capillary clot experiment. **b,** Sequential revisits of damaged capillary niche after laser-induced clot formation in *Csf1r-EGFP* mice. Simultaneous visualization of blood flow before and after clot formation via third harmonic generation (white) from red blood cells (RBC) and intravenous rhodamine dextran (RhDex) (red). Yellow lightning bolt indicates site of laser-induced capillary clot. Yellow arrowheads indicate extra-luminal vascular debris. **c,** Scheme of laser-induced capillary clot in niches with or without CAMs. **d,** Sequential revisits of damaged capillary

niche after laser-induced clot formation in *Csf1r-EGFP;R26-mTmG* mice. Capillary clot formation (yellow lightning bolt) was performed at 940nm for 1s in 10 month old mice. Yellow arrowheads indicate extra-luminal vascular debris. **e,** Quantification of capillary reperfusion at day 1 and 7 after laser-induced clotting (n = 16 capillary clots in regions with CAMs (<75μm from clot), n = 16 capillary clots in regions without CAMs (>75μm from clot; 3 mice in total; capillary reperfusion (with CAMs vs without CAMs) was compared at Day 1 and Day 7 by paired Student's t test; mean ± SD). Scale bar, 50 μm.

Extended Data Figure 6

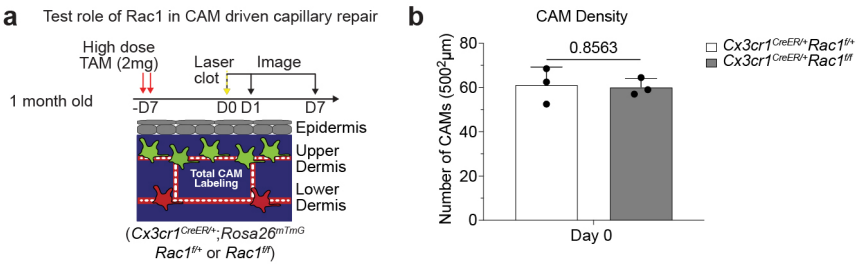

Extended Data Figure 6. CAM density in mice with deficiencies in macrophage phagocytic machinery. a, Scheme of laser-induced capillary clot in *Cx3cr1*^{CreER};*Rac1*$^{fl/fl}$ and *Cx3cr1*^{CreER};*Rac1*$^{fl/+}$ mice. **b,** Quantification of CAM density at Day 7 after laser-induced clotting (n = 3 mice in each group; two 500µm^2 regions per mouse; CAM density (*Rac1*$^{fl/+}$ vs *Rac1*$^{fl/fl}$) was compared at day 0 (same day of clot induction) by unpaired Student's t test; mean ± SD).

Extended Data Figure 7

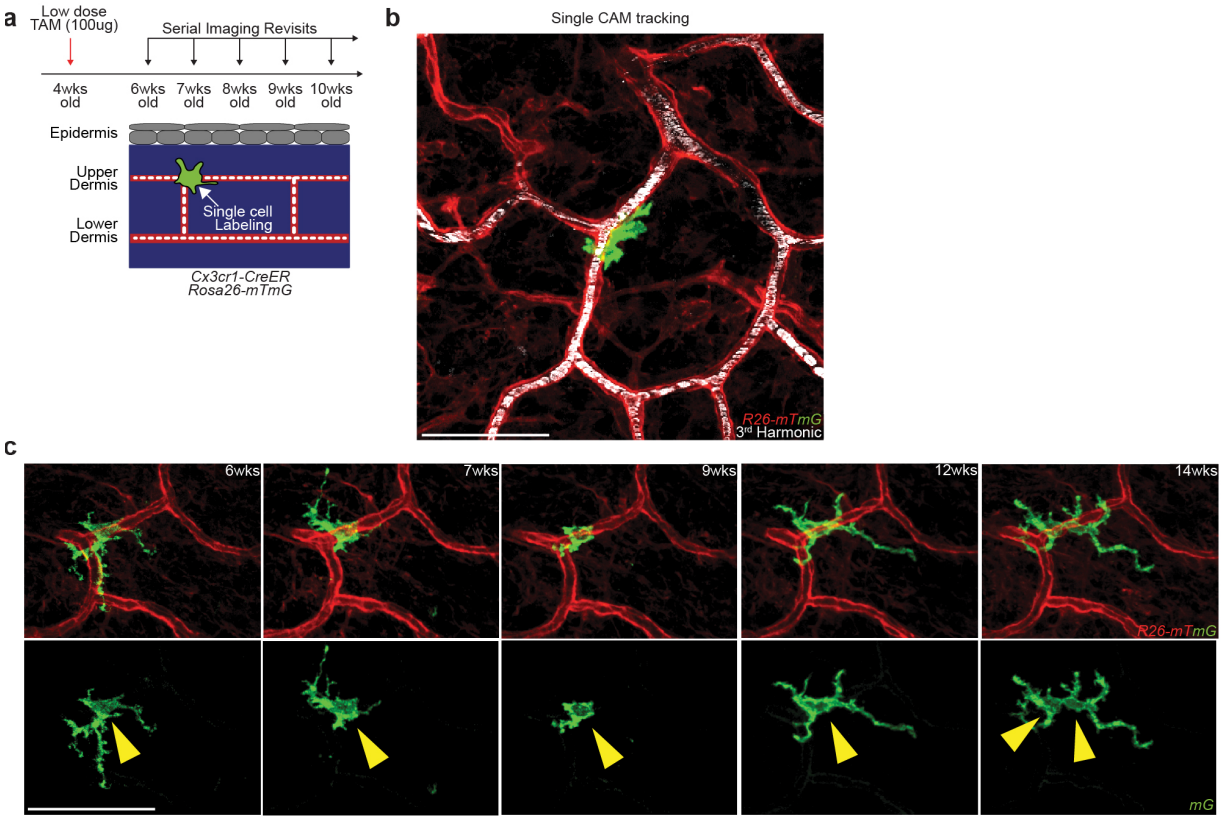

Extended Data Figure 7. Single-cell *in vivo* lineage tracing of resident capillary-asssociated macrophages. a, Scheme of long-term tracking of CAM self-renewal experiment. **b,** Representative image of single macrophage tracing in *Cx3cr1-CreERT2*; *R26-mTmG* mice. **c,** Representative serial revisit images of single macrophage tracing in *Cx3cr1-CreERT2*; *R26-mTmG* mice.

Extended Data Figure 8

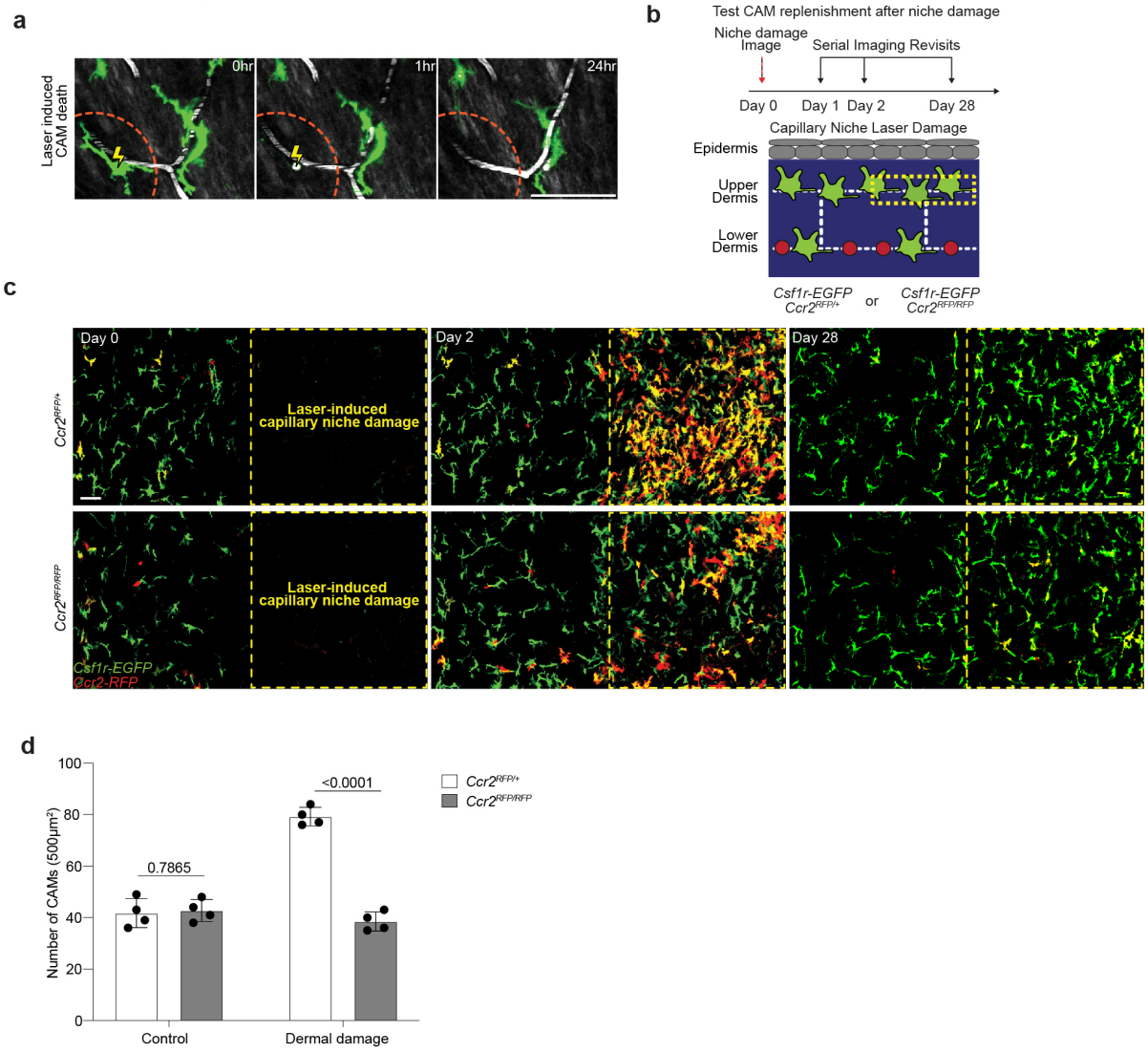

Extended Data Figure 8. Injury-induced replenishment of CAM population is partially CCR2-dependent. a, Representative revisits of CAM replacement after laser-induced CAM ablation in *Csf1r-EGFP* mice. Macrophage laser ablations (yellow lightning bolt) were performed to leave an empty capillary niche (orange dashed line). **b,** Scheme of CAM replacement after capillary niche damage in *Csf1r-EGFP*; *Ccr2*$^{RFP/+}$ or *Ccr2*$^{RFP/RFP}$ mice. **c,** Representative revisits of CAM replacement after a regional laser-induced damage to the capillary niche. **d,** Quantification of replenishment rate (*Csf1r-*

EGFP+ cells) of empty CAM niche after laser-induced CAM loss and niche damage (n = 4 mice per group; two 500μm^2 regions per mouse; CAM density (*Ccr2*$^{RFP/+}$ vs *Ccr2*$^{RFP/RFP}$) was compared by unpaired Student's t test; mean ± SD). Scale bar, 50μm.

Extended Data Figure 9

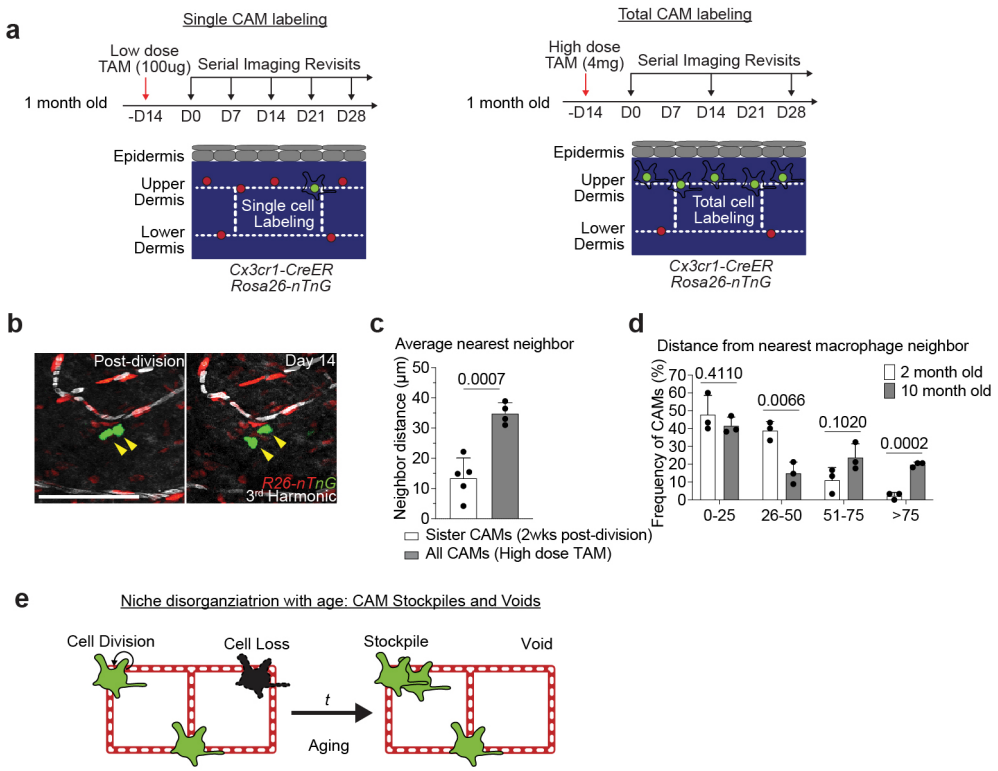

Extended Data Figure 9. Spatially uncoupled proliferation and loss progressively lead to disorganized macrophage niche patterning. a, Scheme of long-term tracking of CAM migration following cell division. **b,** Representative revisits of single macrophage lineage tracing in *Cx3cr1-CreERT2*; *R26-nTnG* mice. Weekly revisits were performed during homeostatic conditions for 5 weeks following a single low-dose intraperitoneal injection of tamoxifen (50µg). **c,** Quantification of neighboring CAM distance of recently divided sister CAMs was compared to total CAM neighboring distance from *Cx3cr1-CreERT2*; *R26-nTnG* mice given a single high-dose intraperitoneal injection of tamoxifen (4mg) (n = 26 sister CAM pairs, from 5 mice in low-dose group; n = 188 CAMs, from 4 mice in high-dose group; Average nearest neighbor distance (2 vs 10 month old) was compared at 0-25, 26-50, 51-75, and >75µm intervals by unpaired Student's t test mean ± SD). **d,** Quantification of distance between nearest CAM

neighbors in 2 and 10 month old *Csf1r-EGFP* mice (n = 90 CAMs in 2 month old mice, n = 101 CAMs in 10 month old mice; 3 mice in each age group; Frequency of CAM distribution (2 vs 10 month old) was compared at 0-25, 26-50, 51-75, and >75μm intervals by unpaired Student's t test; mean ± SD). **e,** Working model of macrophage renewal and organization in the skin aging capillary niche. Scale bar, 50μm.

Extended Data Figure 10

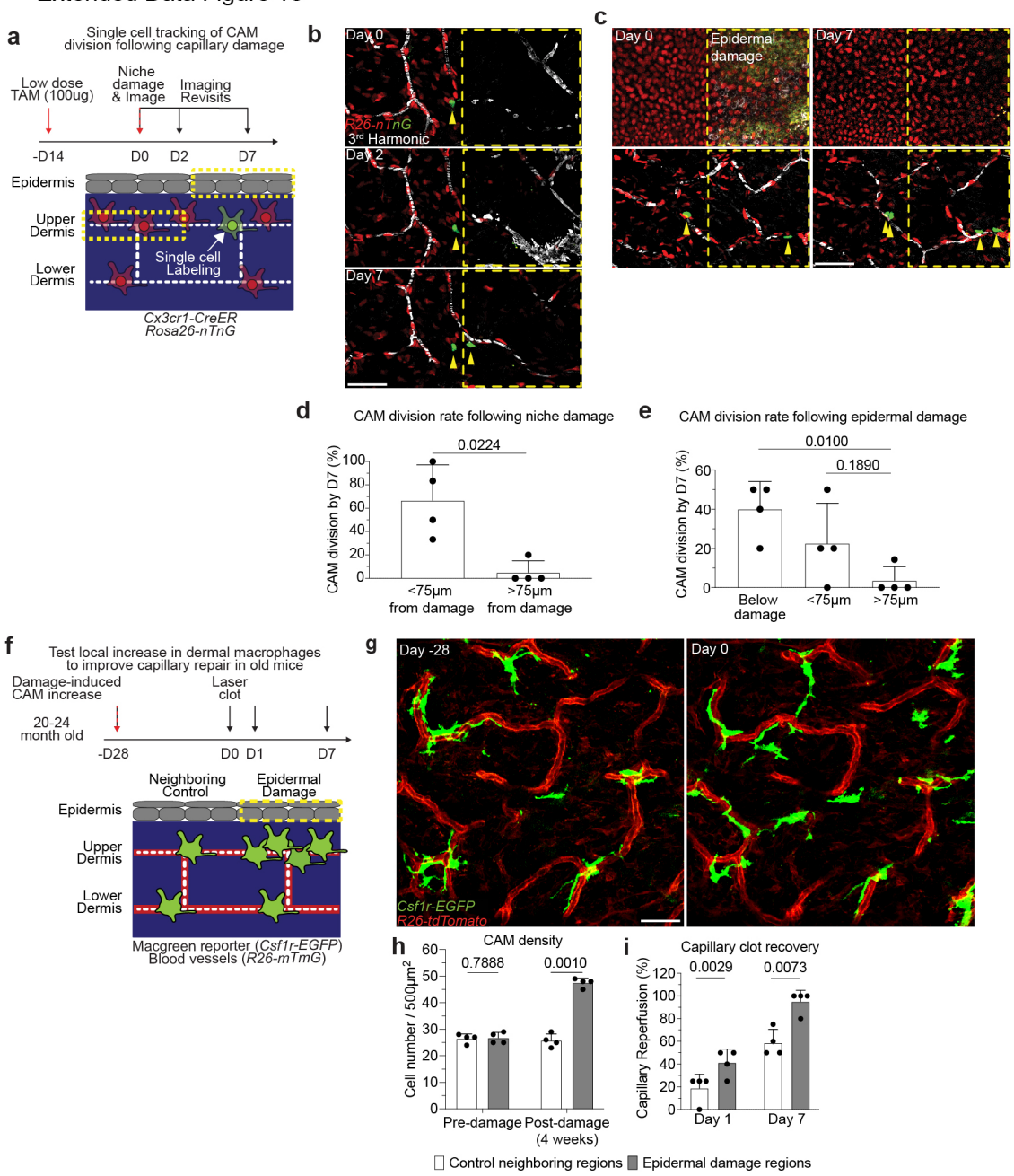

852

853 **Extended Data Figure 10. Large niche damage expands CAM population and**

854 **improves capillary repair in old mice. a,** Scheme of tracking of CAM proliferation

855 following laser-induced damage to nearby capillary or epidermal niches. **b,c,**

856 Representative revisits of single macrophage lineage tracing in *Cx3cr1-CreERT2*; *R26-*

857 *nTnG* mice following (b) capillary and (c) epidermal damage. **d,e,** Quantification of CAM

858 proliferation based on proximity to (d) capillary and (e) epidermal damage (n = 25 CAMs
859 tracked in capillary damage regions, n = 56 CAMs tracked in epidermal damage
860 regions; 4 mice in each group; CAM proliferation (based on damage proximity) was
861 compared at day 7 by paired Student's t test; mean ± SD). **f,** Scheme of local damage-
862 induced expansion of CAMs in the aged capillary niche. **g,** Representative images of
863 CAM density in *Csf1r-EGFP; R26-mTmG* mice 28 days following overlaying epidermal
864 laser damage. **h,** Quantification of CAM density following overlaying epidermal damage
865 (n = 4 mice in total; two 500μm^2 regions for both epidermal damage and control
866 conditions per mouse; CAM density (Epidermal damage vs Control) was compared by
867 paired Student's t test; mean ± SD). **i,** Quantification of capillary reperfusion at day 1
868 and 7 after laser-induced clotting (n = 17 capillary clots in epidermal damage regions, n
869 = 17 capillary clots in neighboring control regions; 4 mice in total; capillary reperfusion
870 (with epidermal damage vs control) was compared at day 1 and day 7 by paired
871 Student's t test; mean ± SD). following laser-induced damage to overlaying epidermal
872 niche. Scale bar, 50μm.
873
874
875
876
877
878
879
880

881 **Supplemental Video Legends**

882

883 **Supplemental Video 1.** Serial optical sections through mouse plantar skin, including
884 epidermis (0-25μm), upper dermis (26-50μm), and lower dermis (51-100μm) in *R26-*
885 *mTmG* (red) mice. Note Second and Third Harmonic Generation illuminates dermal
886 collagen (blue) and red blood cells (white), respectively. Scale bar, 50μm.

887

888 **Supplemental Video 2.** Serial optical sections through mouse plantar skin, including
889 epidermis (0-15μm), upper dermis (16-40μm), and lower dermis (41-52μm) in *Csf1r-*
890 *EGFP* mice. Note distinct macrophage (green) density and morphology in each tissue
891 niche. Scale bar, 50μm.

892

893 **Supplemental Video 3.** Time-lapse recording of capillary blood flow via third harmonic
894 generation (white) from red blood cells and intravenous rhodamine dextran (red) in
895 *Csf1r-EGFP* mice. Note some capillary segments show obstructed red blood cell and
896 rhodamine dextran flow. Scale bar, 50μm.

897

898 **Supplemental Video 4.** Serial optical sections through upper dermal capillary niche in
899 *Cx3cr1-GFP; R26-mTmG* mice. Note macrophage (green) localization and morphology
900 around capillary (red) network. Scale bar, 50μm.

901

902 **Supplemental Video 5.** Time-lapse recording of capillary blood flow in *Cx3cr1-CreER;*
903 *R26-mTmG* mice. Note inconsistent and obstructed blood flow (white) in capillary (red)
904 segments without associated macrophages (green). Scale bar, 50μm.
905
906 **Supplemental Video 6.** Time-lapse recording following laser-induced capillary clot
907 formation in *Csf1r-GFP; R26-mTmG* mice. Note rapid migration of neighboring capillary-
908 associated macrophages (green) toward site of clot formation (yellow arrowhead). Scale
909 bar, 50μm.
910